Proceedings of the Pakistan Academy of Sciences: A Physical and Computational Sciences 62(3): 221-233 (2025)
Copyright © Pakistan Academy of Sciences
ISSN (Print): 2518-4245; ISSN (Online): 2518-4253
http://doi.org/10.53560/PPASA(62-3)701

Pakistan Academy of Sciences

Research Article

Formaldehyde Pollution in Ahvaz, Iran: Spatiotemporal Trends and Health Risks

Faezeh Borhani[1*], Mohammad Hashemzadeh[1], Samira Andam[2], and Seyed Mohsen Mousavi[3]

[1]Department of Environmental Engineering, Faculty of Civil and Environmental Engineering, Tarbiat Modares University, Tehran 1411713116, Iran

[2]Department of Life Science Engineering, Faculty of New Sciences and Technologies, University of Tehran, Tehran 143951561, Iran

[3]Department of Environmental Planning and Design, Shahid Beheshti University, Tehran 1983969411, Tehran, Iran

Abstract: We present a satellite-driven, four-year assessment of formaldehyde (HCHO) over Ahvaz that quantifies its spatiotemporal variability, meteorological controls, and health risk. Using Sentinel-5P/TROPOMI (2019–2022) together with MERRA-2/GLDAS/AIRS fields, we relate HCHO to co-pollutants (CO, NO_2, SO_2) and meteorology (precipitation, temperature, wind speed, relative humidity, dew point) and map hotspots via IDW; health risks are evaluated with RAIS. HCHO correlates positively with temperature ($r = 0.92$) and negatively with relative humidity ($r = -0.84$) and precipitation ($r = -0.65$); the wind-speed link is moderately positive ($r = 0.46$), with primary co-pollutants are weak (CO: $r \approx 0.08$; NO_2: $r \approx -0.02$). Interannually, 2020 shows the highest HCHO and 2021 the lowest (annual mean ≈8% lower in 2021), with persistent hotspots along the southeastern industrial corridor. IUR-based lifetime inhalation cancer risk peaks in 2020 at ~506 expected excess cases citywide and is lowest in 2021 at ~468. These quantitative results highlight temperature-driven photochemistry and moisture-related removal as key controls on HCHO and motivate strengthened air-quality management to mitigate exposure and protect public health in Ahvaz.

Keywords: Formaldehyde (HCHO), Air Pollutants, Meteorological Conditions, Sentinel-5P, Spatiotemporal, Health Risk Assessment.

1. INTRODUCTION

Ahvaz has been identified as a critical area for air quality research due to its high levels of various pollutants, including Formaldehyde (HCHO), ozone (O_3), nitrogen dioxide (NO_2), and sulfur dioxide (SO_2), and carbon monoxide (CO). The city's geographical and climatic conditions exacerbate pollution levels, leading to severe health impacts among residents. Notably, studies have shown that exposure to these pollutants correlates with increased hospital admissions for cardiovascular diseases and respiratory issues [1-3]. Statistical data indicate that, following Tehran and Isfahan, Ahvaz ranks third in terms of air pollution levels in Iran, and this condition is on a continuous upward trajectory. Consequently, it is essential to examine the trends of air pollutants in Ahvaz city. HCHO represents a significant member of the aldehyde family, prevalent in both indoor and outdoor atmospheric environments. This compound is critical for assessing atmospheric oxidation capacity due to its toxic, irritating, and flammable properties [4, 5]. Epidemiological studies investigating the health impacts of HCHO have led the U.S. National Toxicology Program and the International Agency for Research on Cancer to classify this gas as a potential contributor to leukemia [6]. HCHO is primarily emitted from anthropogenic activities such as vehicular emissions, industrial processes,

Received: June 2025; Revised: August 2025; Accepted: September 2025
* Corresponding Author: Faezeh Borhani <f.borhani@modares.ac.ir>

and the use of certain household products. In urban environments like Ahvaz, traffic-related emissions are significant contributors to ambient HCHO levels. Furthermore, photochemical reactions can lead to secondary formation of HCHO from other pollutants, complicating efforts to manage air quality.

Existing research indicates that meteorological parameters and precursor pollutants substantially influence variations in atmospheric pollutant concentrations, as well as the assessment of associated health risks across different months and seasons [7-9]. Borhani *et al.* [10] conducted a pivotal study investigating the effects of fine particulate matter ($PM_{2.5}$) on air quality and public health in Tehran, Iran, over a ten-year period from 2011 to 2020. The research analyzed $PM_{2.5}$ concentrations, the Air Quality Index (AQI), and hospital admissions associated with chronic obstructive pulmonary disease (COPD) linked to $PM_{2.5}$ exposure. The results revealed that reductions in $PM_{2.5}$ levels can yield significant health benefits. Another study examined both indoor and outdoor concentrations of BTEX compounds in Tehran, emphasizing how building characteristics can influence exposure levels. This research suggests that urban planning and building design could mitigate exposure risks to these toxic pollutants [11]. Dehghani *et al.* [12] conducted an evaluation of HCHO concentrations in the ambient air of Tehran, revealing significant levels that may pose health risks. The results underscore the necessity for immediate interventions to regulate emissions from both industrial and vehicular sources to safeguard public health. Hedayatzadeh and Hassanzadeh [13] examined benzene, toluene, ethylbenzene, and xylene (BTEX) compounds in Ahvaz's urban atmosphere, assessing their prevalence, sources, and health risks. Their study underscored the health threats posed by these VOCs, which contribute to air pollution. The findings emphasizes the need for effective air quality management in urban areas like Ahvaz, highlighting the importance of monitoring BTEX levels to mitigate health risks and guide policy on emissions and traffic.

While the relationship between HCHO and various atmospheric variables has been explored, fewer studies have undertaken a comprehensive assessment that simultaneously considers precursor pollutants and a full suite of meteorological conditions . This is particularly true for specific, under-examined urban hotspots, where such detailed analyses are crucial for developing effective, localized mitigation strategies. Ahvaz, despite its status as one of Iran's most critical air pollution centers, has been notably overlooked in existing research. This study addresses this significant gap by conducting a multi-faceted analysis of HCHO's spatiotemporal behavior in Ahvaz from 2019 to 2022 and systematically correlating it with key atmospheric variables. Building upon this essential groundwork, the paper's primary contribution is the quantification of direct public health consequences using the RAIS framework. This approach not only characterizes the pollutant's dynamics in a high-risk environment but also translates these findings into tangible human health impacts, with results presented at both urban and district scales.

2. MATERIALS AND METHODS

2.1. Study Area

Ahvaz ($31^{\circ}30'N$ and $48^{\circ}65'E$) serves as the capital of Khuzestan province in southwestern Iran, is divided into eight districts (Figure 1 and Table 1). The city is situated on both banks of the Karun River and is characterized by a low range of sandstone hills. Covering an area of 318 square kilometers, Ahvaz ranks among the largest cities in Iran, holding the third position in terms of size, following Tehran and Mashhad. Positioned within the Khuzestan plains, the city is approximately 12 meters above sea level. The average annual precipitation in Ahvaz ranges from 220 to 250 mm, with minimum temperatures recorded at 5

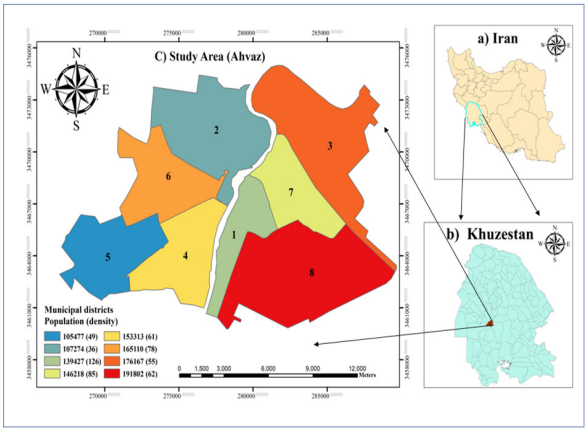

Fig. 1. The location of the study area, (a) Iran, (b) Khuzestan province, and (c) Ahvaz city.

Table 1. Population and area of Ahvaz city by Municipal districts.

Municipal districts	Land use	Area (Hectare)	Population (People)	Population density
1	Including the central and historical parts of the city	1103	139427	126
2	Residential and commercial areas with access to urban facilities	2913	107274	36
3	Including industrial and economic areas	3181	176167	55
4	Residential areas with a focus on infrastructure development	2527	153313	61
5	Includes new neighborhoods and housing projects	2155	105477	49
6	Cultural and recreational areas	2111	165110	78
7	Marginal and less developed regions	1719	146218	85
8	Including special areas and large urban projects	3098	191802	62
Total		19494	1184788	

C and maximum temperatures exceeding 40 °C. The average relative humidity typically fluctuates between 14% and 58%, while the average annual wind speed is approximately 38 kilometers per hour. Given its geographical and industrial significance, Ahvaz plays a crucial role in the economic and industrial landscape of the country.

2.2. Datasets and Preparation

2.2.1. Sentinel-5P (TROPOMI) data retrieval and preparation

Spatio-temporal maps of HCHO concentrations and other air pollutants (CO, NO_2, O_3, SO_2) are instrumental in identifying emission hotspots and assessing the effectiveness of pollution mitigation strategies over time. (The units for HCHO, CO, NO_2, and SO_2 are given as vertical column density (VCD) in mol m^{-2}, while O_3 is measured as total column density in Dobson Units (DU). This study analyses the average daily total air pollutants column density obtained from the Sentinel-5P satellite, specifically utilizing the TROPOMI (Tropospheric Monitoring Instrument Sentinel-5 Precursor) HCHO monitoring instrument, accessible through the Google Earth Engine (GEE) cloud platform [14]. We used Level-2 OFFL products and retained only pixels with (qa_value ≥ 0.5.) The data spans from January 1, 2019, to December 31, 2022, covering a four-year period. TROPOMI operates with a spectral resolution ranging from 0.25 to 0.55 nanometre (nm) and provides global daily coverage with a spatial resolution of 5.5 × 3.5 km, (commonly reported as ~3.5 × 5.5 km at nadir). Following the acquisition and importation of the data into Quantum GIS (QGIS), the Inverse Distance Weighting (IDW) method was employed to generate monthly HCHO (total column) maps [15].

In addition, for subsequent health risk assessment (RAIS), HCHO needs to be expressed as volumetric concentration (μg m^{-3}). Therefore, the satellite-retrieved VCD of HCHO (VCD, mol m^{-2}) was converted to volumetric concentration using the following relation:

$$Concentration(original)_{\left(\frac{\mu g}{m^3}\right)} = \frac{C_{\left(\frac{mol}{m^2}\right)} \times Molar\ mass\ \left(\frac{g}{mol}\right)}{H(m)} \times 10^6 \quad (1)$$

Where, C denotes the HCHO ($mol.m^{-2}$) and the molar mass of HCHO is 30.026 $g.mol^{-1}$. In general, the denominator H represents the planetary boundary layer height (PBLH). In this study, for simplicity, we assume H = 1000 (m), which is a reasonable approximation.

2.2.2. Data collection of meteorological parameters using the NASA Giovanni

Meteorological parameter (i.e., total precipitation rate (PR), surface air temperature (T), relative humidity (RH), surface wind speed (WS), dew point temperature (DWP)) data were sourced from the MERRA-2, GLDAS, and AIRS satellite models through the Giovanni platform (Table 2). The Giovanni platform functions as an online interactive geographic visualization tool, facilitated by NASA's Goddard Earth Science Data and Information Service (GES DISC) [16, 17].

Table 2. Summary of meteorological parameters used in this study.

No.	Parameter	Unit	Source	Temporal Resolution	Spatial Resolution	Begin Date	End Date	Abbreviation Name
1	Total precipitation rate	$\frac{kgr}{m^2 s}$	GLDAS Model	Monthly	1°×1°	01/01/2000	31/12/2023	GLDAS_NOAH10_M v2.1
2	Surface air temperature	K	MERRA-2 Reanalysis	Monthly	0.5°×0.625°	01/01/1980	29/02/2024	M2TMNXFLX v5.12.4
3	Relative Humidity at Surface (Daytime/Ascending, AIRS-only)	Percent ($\%$)	AIRS	Monthly	1°×1°	01/09/2002	29/02/2024	AIRS3STM v7.0
4	Surface wind speed	$\frac{m}{s}$	MERRA-2 Reanalysis	Monthly	0.5°×0.625°	01/01/1980	29/02/2024	M2TMNXFLX v5.12.4
5	2-meter dew point temperature	K	MERRA-2 Reanalysis	Monthly	0.5°×0.625°	01/01/1980	29/02/2024	M2TMNXSLV v5.12.4

MERRA-2: Modern-Era Retrospective Analysis and Research and Application-version 2 product, GLDAS: Global Land Data Assimilation System, AIRS: Atmospheric Infrared Sounder.

2.2.3. Health risk assessment

The RAIS is a comprehensive tool developed under the supervision of the U.S. Department of Energy (DOE) since 1996. It serves as a resource for assessing environmental risks, particularly concerning pollutants like HCHO. The system focuses on various dimensions of exposure, including contact duration, application duration, and contact frequency, which are critical for evaluating how individuals interact with hazardous substances [18]. In RAIS terminology, CDI (Chronic Daily Intake) denotes a dose normalized by body weight and time (typically μg ·kg^{-1}·day^{-1}).

To assess CDI of a pollutant, RAIS utilizes specific formulas based on the type of exposure. The CDI can be calculated in two primary ways: Contact CDI: This is expressed in $\frac{\mu g}{m^3}$ and considers the duration and frequency of exposure (Equation 2). In practice, Eq. (2) provides a time-averaged ambient concentration used later as the concentration term in the IUR-based risk (Eq. 4).

Inhalation CDI: For inhalation exposure, the pollutant concentration in the air is measured in μg/m³. This approach specifically addresses the risks associated with airborne pollutants (Equation 3). In Eq. (3), CDI is a dose-based quantity (mg·kg^{-1}·day^{-1}) that uses breathing rate and body weight.

$$CDI_{(\frac{\mu g}{m^3})} = \frac{C_{(\frac{\mu g}{m^3})} \times ED_{(days)}}{AT_{(days)}} \quad (2)$$

$$CDI_{(\frac{\mu g}{kg-day})} = \frac{C_{(\frac{\mu g}{m^3})} \times ED_{(days)} \times BR_{(\frac{m^3}{day})}}{BW_{(kg)} \times AT_{(days)}} \quad (3)$$

Where, *C* and *ED* are the concentration and exposure duration, *AT* is the average human lifespan (typically considered to be 70 years for cancer risk assessments), *BR* is the breathing rate, and *BW* is the average body weight (often considered to be around 70 kg (approximately 154 lbs) for adults).

2.2.3.1. Cancer risk assessment

Cancer risk assessment involves evaluating the likelihood of developing cancer based on various factors, including exposure to carcinogens. The methodology typically incorporates concepts such as cancer slope factors and respiratory risk units, which are often linear and suggest that there is no safe threshold for exposure-meaning even the lowest concentration of a carcinogen can increase cancer risk.

The following equation is used to calculate the cancer risk associated with exposure to a specific carcinogen.

$$Risk\ (unitless) = CDI\ \left(\frac{\mu g}{m^3}\right) \times IUR\ \left(\frac{\mu g}{m^3}\right)^{-1} (4)$$

$$Risk\ (unitless) = CDI\ \left(\frac{\mu g}{kg.day}\right) \times CSF\ (\frac{\mu g}{kg.day})^{-1} (5)$$

The Inhalation Unit Risk (IUR) is a measure of the potency of the carcinogen. It represents the upper-bound probability of an individual developing cancer as a result of continuous exposure to the carcinogen at a concentration of 1 $\frac{\mu g}{m^3}$ in air over a lifetime. The IUR is expressed as the inverse of the concentration $\left(\frac{\mu g}{m^3}\right)^{-1}$. Also, Cancer Slope Factor (CSF) is a toxicological measure that quantifies the risk of cancer associated with exposure to a carcinogen. It is expressed in units of risk per unit of exposure $(\frac{\mu g}{kg.day})^{-1}$. The CSF indicates the increase in cancer risk per unit of CDI and is specific to each carcinogen [19, 20].

2.2.4. Matrix heatmap of data

Heatmaps function as a highly effective visualization instrument that is particularly useful for representing data organized in a matrix format. This technique employs variations in color to illustrate different values within the dataset. In the context of this study, this visualization method was specifically applied to clarify the relationship between concentrations of HCHO, other air pollutants (CO, NO_2, O_3, SO_2) and various meteorological parameters observed from the years 2019 to 2022. The heatmaps utilized in this research were created through the use of the seaborn heatmap functionality available in Python, which relies on the capabilities of the NumPy library to facilitate the data processing and visualization [21].

3. RESULTS AND DISCUSSION

The monthly average of air pollutants concentrations

Table 3. The monthly average HCHO in Ahvaz City (VCD and converted volumetric).

Year		Winter			Spring			Summer			Autumn		
		Jan	**Feb**	**Mar**	**Apr**	**May**	**Jun**	**Jul**	**Aug**	**Sep**	**Oct**	**Nov**	**Dec**
2019	$\frac{mol}{m^2}$	0.00005	0.0001178	0.000104	0.00014	0.000178	0.000226	0.00023	0.000258	0.000193	0.000188	0.000164	0.000087
	$\frac{\mu g}{m^3}$	0.0017612	0.0041484	0.0036634	0.0049174	0.0062616	0.0079538	0.0081077	0.0090884	0.0068093	0.0066223	0.0057635	0.0030646
2020	$\frac{mol}{m^2}$	0.0000886	0.0000868	0.0001208	0.000138	0.000194	0.000206	0.00027	0.000229	0.000263	0.00019	0.000151	0.000083
	$\frac{\mu g}{m^3}$	0.0031209	0.0030575	0.0042552	0.0048434	0.0068336	0.0072588	0.0095213	0.0080813	0.0092479	0.0067101	0.0053309	0.0029237
2021	$\frac{mol}{m^2}$	0.0001243	0.000087	0.0000848	0.000148	0.000203	0.000198	0.000216	0.00023	0.000179	0.00014	0.000144	0.000116
	$\frac{\mu g}{m^3}$	0.0043798	0.0030646	0.0029871	0.0052193	0.0071436	0.0069728	0.0076209	0.0081183	0.00629154	0.0049188	0.0050773	0.0040731
2022	$\frac{mol}{m^2}$	0.000074	0.0000901	0.0000855	0.00012	0.000144	0.000196	0.000246	0.00028	0.000236	0.000184	0.00015	0.000101
	$\frac{\mu g}{m^3}$	0.0026066	0.0031737	0.0030117	0.0042129	0.0050837	0.0069171	0.0086551	0.0098782	0.0083106	0.0064919	0.0052894	0.0035535

and meteorological variables from 2019 to 2022 in Ahvaz city is presented in Appendix, Table A.

3.1. Temporal and Spatial Variation of the HCHO and other Air Pollutants (CO, NO_2, O_3, SO_2)

This study examines the atmospheric pollutants concentrations in Ahvaz city. The measured HCHO concentrations throughout the four-year study period consistently fall below the standard parts per billion (ppb) threshold and remain within acceptable limits across all months (Table 3). Figure 2 shows the spatial distribution of the average annual values of the Sentinel-5P total column density of HCHO ($\frac{mol}{m^2}$) in Ahvaz city from January 1, 2019 to December 31, 2022.

The maximum and minimum monthly average values of total HCHO were recorded in August at 0.000249583 $\frac{mol}{m^2}$ and in January at 0.000084235 $\frac{mol}{m^2}$ respectively (Table 3). Overall, HCHO emissions exhibit seasonal variability, with concentrations generally higher in summer than in winter [22]. In unpolluted outdoor air, HCHO concentrations are typically below 1 ppb, whereas urban environments have reported concentrations ranging from 1 to 25 ppb [23, 24]. This study has indicated that regions 3, 6, 7, and 8 experience the highest levels of HCHO emissions. This situation raises significant public health concerns, necessitating targeted interventions to improve air quality in these areas. The high emissions can be attributed to factors such as urbanization, industrial activities, and traffic density, which are prevalent in these regions (Table 1).

The total CO concentration reached its peak in region 8 during the period from 2019 to 2021, while region 1 exhibited the highest level in 2022 (Figure 3(a-c)). In Ahvaz, the maximum average CO concentration was recorded in August, whereas the minimum was noted in November (Figure 3(d)). The highest average concentration of NO_2 in Ahvaz was recorded in January, while the lowest concentration occurred in April. These findings underscore the significance of seasonal changes on air quality in Ahvaz. The data indicates that both CO and NO_2 levels are influenced by meteorological conditions, traffic patterns, and seasonal activities. The total O_3 concentration is greatest in regions 2,

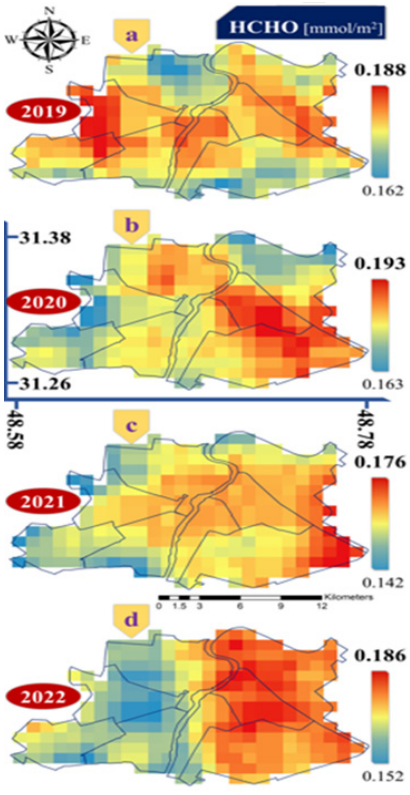

Fig. 2. The spatial distribution of the average annual concentrations of HCHO in Ahvaz, Iran from 2019 to 2022.

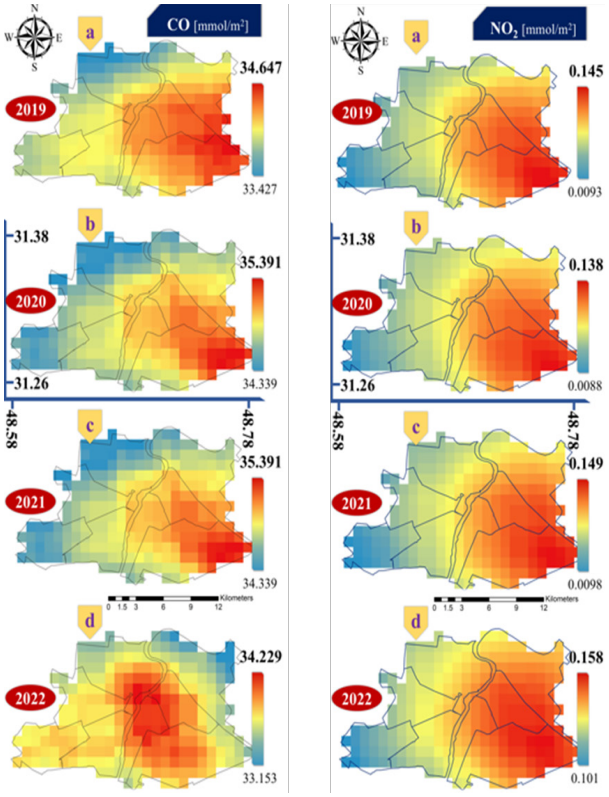

Fig. 3. The spatial distribution of the average annual concentrations of CO and NO_2 in Ahvaz, Iran from 2019 to 2022.

5, and 6, while the highest concentration of SO_2 is observed in region 8 (Figure 4). Figure 4 shows persistent spatial gradients: O_3 remains higher over the northwest–central districts and lower toward the southeast in all four years, with a slight citywide increase from 2019 to 2022. In contrast, SO_2 displays stronger spatial contrasts with recurrent hotspots in the eastern/southeastern industrial corridor (notably region 8) and comparatively lower values in the northwest. Year-to-year variability is larger for SO_2 than for O_3, consistent with episodic emission/stack operations. These patterns suggest regionally driven photochemistry and NO_x titration for O_3, versus more local combustion/industrial sources for SO_2.

3.2. Statistical Associations between HCHO, Meteorology, and Co-Pollutants

Figure 5 summarizes the co-variation between meteorology and pollutants. The HCHO-temperature linkage is very strong (r = 0.92; see also Figure. 6(a)), consistent with temperature-driven VOC emissions, faster photochemistry, and a deeper daytime boundary layer that sustains secondary carbonyl formation; this pattern matches earlier satellite evidence for warm-season enhancement [25, 26]. In contrast, relative humidity shows a pronounced negative association with HCHO (r = -0.84; Figure 6(b)): higher RH generally promotes wet removal/aqueous uptake and reduces actinic flux, both of which diminish HCHO [27]. A similar damping appears for precipitation (PP) (r = -0.65), reflecting washout and cloud shielding [27].

Wind acts in two ways. The HCHO-WS correlation is moderately positive (r = 0.46), implying that stronger winds can deepen/mix the boundary layer and transport VOC-NO_x precursors that maintain secondary HCHO. At the same time, WS-NO_2/SO_2 correlations are negative (-0.35 and -0.70), evidencing efficient dispersion of primary combustion pollutants [28]. The modest/negative HCHO-O_3 correlation (≈ -0.23) is compatible with local NO_x titration of O_3 in traffic-influenced areas, which can decouple O_3 from HCHO despite shared photochemical drivers.

Finally, the small HCHO correlations with CO (0.08) and NO_2 (-0.02) indicate that satellite columns of primary pollutants do not always track a secondary product at monthly scales, owing to differences in sources, chemistry, and mixing height. Overall, temperature favor higher HCHO, whereas humidity and precipitation suppress it, yielding the coherent pattern evident in Figure 5.
For completeness, Figure 6 makes these links explicit in the time domain: Figure 6(a) shows monthly HCHO and surface-air temperature (2019-2022) evolving in phase, with co-located summer maxima (typically July-August) and winter minima

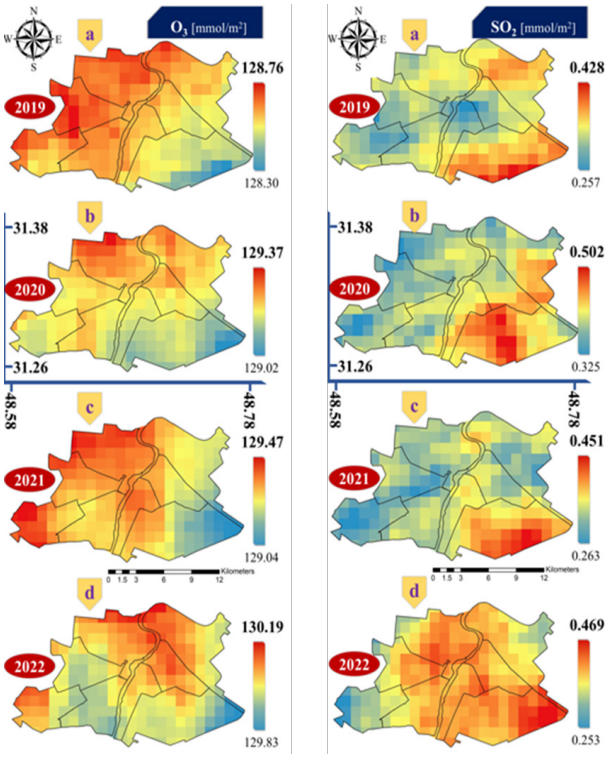

Fig. 4. The spatial distribution of the average annual concentrations of O_3 and SO_2 in Ahvaz, Iran from 2019 to 2022.

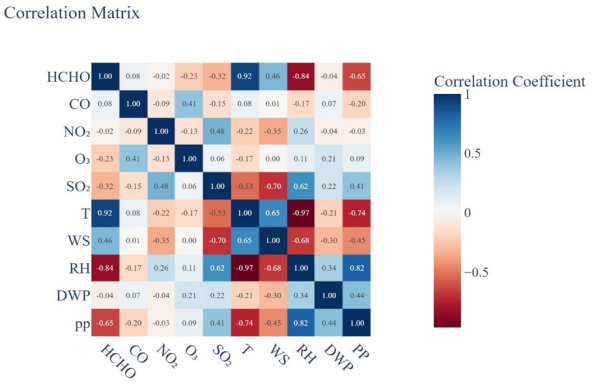

Fig. 5. Heatmap and summary of Spearman's rank coefficient for correlations between monthly average HCHO, other air pollutants (CO, NO_2, O_3, SO_2) and Meteorological parameters (T, WS, RH, DWP, PP) in Ahvaz, Iran, from 2019 to 2022.

(November-January). Figure 6(b) displays the anti-phase behavior with RH, where cool-season humidity peaks and summer troughs mirror the negative correlation noted above. Together, Figures 5 and 6 reinforce that temperature-driven photochemistry and VOC emissions elevate HCHO, while humidity/precipitation primarily act via removal and reduced photolysis.

3.3. Result of Health Risk Assessment

According to the 2015 census data from the Iran Statistics Center, the population of Ahvaz city was 1,184,788 individuals [29]. The values for contact risk and respiratory risk from 2019 to 2022 are presented in Table 4; for context, population-scaled counts (risk × city population) are also reported.

The findings indicate that respiratory risk is consistently ~462 times higher than contact risk across all years, reflecting inhalation as the dominant exposure pathway. Citywide expected cases vary from ~468 (2021) to ~506 (2020), closely tracking the annual mean HCHO (highest in 2020, lowest in 2021). These interannual differences are consistent with the concentration patterns reported in Section 3.2. The reported risks are unitless lifetime cancer probabilities per individual (IUR applied to the annual-mean EC under the assumption of chronic exposure). The accompanying counts represent the expected number of excess cases obtained by scaling the risk by the city population.

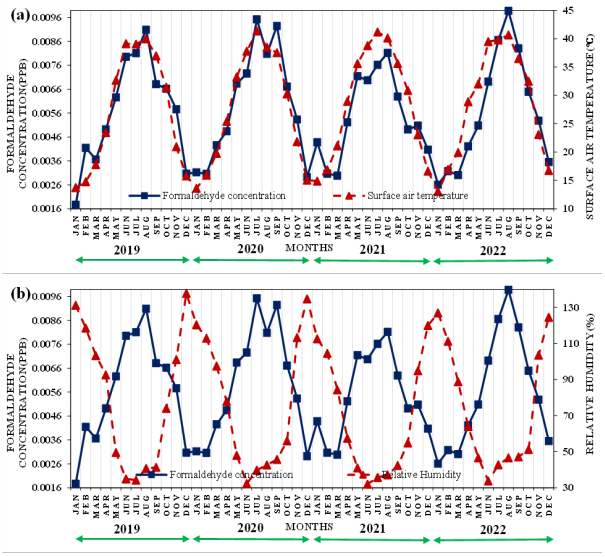

Fig. 6. Comparison of monthly average of HCHO concentrations and (a) Surface air temperature and (b) Relative Humidity, from 2019 to 2022.

4. CONCLUSIONS

This study quantified 2019-2022 spatiotemporal variability of HCHO over Ahvaz using Sentinel-5P/TROPOMI, examined its associations with meteorological drivers (PP, WS, T, RH, DWP) and co-pollutants (CO, NO_2, O_3, SO_2), and evaluated health risks via RAIS.

- We find marked seasonal and spatial variability in HCHO, SO_2, NO_2, O_3, and CO. Temperature shows a strong positive link with HCHO, while relative humidity and precipitation are negatively associated, consistent with enhanced photochemistry at higher T and wet removal/cloud shielding at higher RH/PP; these patterns agree with prior studies [30, 31].
- Spatial contrasts persist across years: O_3 concentrations/columns are generally higher in the western–northwestern districts, whereas SO_2 exhibits recurrent hotspots in Region 8, reflecting localized industrial/combustion influences versus regionally driven photochemistry for O_3.
- Health risk: inhalation (respiratory) lifetime cancer risk clearly exceeds contact risk in all years. The highest respiratory risk occurs in 2020 and the lowest in 2021, mirroring the corresponding annual mean HCHO.

Table 4. Annual risk assessment of HCHO in Ahvaz city from 2019 to 2022.

Year	Total annual concentration	Average annual concentration	Annual contact risk	Annual respiratory risk	Risk person per year (population of Ahvaz 1,184,788)	
					Annual contact risk/population	Annual respiratory risk/population
2019	0.001935	0.00016125	8.861E-07	0.00040897	1.05	484.5
2020	0.0020209	0.00016841	9.254E-07	0.00042711	1.10	506.03
2021	0.0018699	0.00015583	8.5628E-07	0.0003952	1.01	468.23
2022	0.0019073	0.00015894	8.734E-07	0.00040311	1.03	477.6

It is worth noting, these results carry uncertainties arising from satellite retrieval and processing (QA/cloud screening and spatial resolution), the conversion from VCD to volumetric concentration (dependence on boundary-layer height), and toxicity parameters/assumptions in RAIS (IUR/CSF ranges and chronic-exposure assumptions). Accordingly, risk values should be interpreted as indicative magnitudes rather than exact counts. The findings underscore the necessity for effective air quality management and monitoring systems in Ahvaz city. Addressing these pollution challenges is crucial for improving living conditions and safeguarding public health against the backdrop of industrialization and environmental factors.

5. Appendix

Table A presents monthly average of HCHO, other air pollutants (CO, NO_2, O_3, SO_2) and meteorological parameters recorded from 2019 to 2022 in Ahvaz, Iran.

6. ACKNOWLEDGEMENTS

Special thanks are extended to the Remote Sensing Laboratory, Faculty of Civil and Environmental Engineering, Tarbiat Modares University, Iran, for their effective assistance in providing the database for this study.

7. ETHICAL STATEMENT

The authors declare that they agree with the publication of this paper in this journal.

8. CONFLICT OF INTEREST

The authors declare that they have no known competing financial interests or personal relationships that could have appeared to influence the work reported in this paper.

9. REFERENCES

1. A. Bhatnagar. Environmental cardiology: studying mechanistic links between pollution and heart disease. *Circulation Research* 99(7): 692-705 (2006).
2. Y. Zhang, Y. Yang, X. He, P. Yang, T. Zong, P. Sun, R. Sun, T. Yu, and Z. Jiang. The cellular function and molecular mechanism of formaldehyde in cardiovascular disease and heart development. *Journal of Cellular and Molecular Medicine* 25(12): 5358-5371 (2021).
3. S.H. Borsi, G. Goudarzi, G. Sarizadeh, M. Dastoorpoor, S. Geravandi, H.A. Shahriyari, Z.A. Mohammadi, and M.J. Mohammadi. Health endpoint of exposure to criteria air pollutants in ambient air of on a populated in Ahvaz City, Iran. *Frontiers in Public Health* 10: 869656 (2022).
4. C. Hak, I. Pundt, S. Trick, C. Kern, U. Platt, J. Dommen, C. Ordóñez, A.S. Prévôt, W. Junkermann, C. Astorga-Lloréns, and B.R. Larsen. Intercomparison of four different in-situ techniques for ambient formaldehyde measurements in urban air. *Atmospheric Chemistry and Physics* 5(11): 2881-2900 (2005).
5. F.M. Onyije and O.G. Avwioro. Excruciating effect of formaldehyde exposure to students in gross anatomy dissection laboratory. *The International Journal of Occupational and Environmental Medicine* 3(2): 92-95 (2012).
6. Y. Zhang, X. Liu, C. McHale, R. Li, L. Zhang, Y. Wu, X. Ye, X. Yang, and S. Ding. Bone marrow injury induced via oxidative stress in mice by inhalation exposure to formaldehyde. *Plos One* 8(9): e74974 (2013).
7. M. Delikhoon, M. Fazlzadeh, A. Sorooshian, A.N. Baghani, M. Golaki, Q. Ashournejad, and A. Barkhordari. Characteristics and health effects of formaldehyde and acetaldehyde in an urban area in Iran. *Environmental Pollution* 242(Part A): 938-951 (2018).
8. A.H. Khoshakhlagh, M. Mohammadzadeh, P. Sicard, and U. Bamel. Human exposure to formaldehyde and health risk assessment: a 46-year systematic literature review. *Environmental Geochemistry and Health* 46(6): 206 (2024).
9. S.M. Mousavi, N.M. Dinan, S. Ansarifard, G. Darvishi, F. Borhani, and A. Naghibi. Assessing the impact of global carbon dioxide changes on atmospheric fluctuations in Iran through satellite data analysis. *Journal of Water and Climate Change* 15(6): 2774-2791 (2024).
10. F. Borhani, M.S. Motlagh, A.H. Ehsani, and Y. Rashidi. Evaluation of short-lived atmospheric fine particles in Tehran, Iran. *Arabian Journal of Geosciences* 15(16): 1398 (2022).
11. M. Hadei, P.K. Hopke, M. Rafiee, N. Rastkari, M. Yarahmadi, M. Kermani, and A. Shahsavani. Indoor and outdoor concentrations of BTEX and formaldehyde in Tehran, Iran: effects of building characteristics and health risk assessment. *Environmental Science and Pollution Research* 25(27): 27423-27437 (2018).

12. M.H. Dehghani, M. Salari, K. Naddafi, S. Nazmara, E. Ahmadi, and P. Kumar. Evaluation of formaldehyde concentration in the ambient air of a most populated Iranian city, Tehran. *Air Quality, Atmosphere & Health* 10(6): 763-772 (2017).
13. F. Hedayatzade and N. Hassanzadeh. Occurrence, probable source, and health risk assessment of benzene, toluene, ethylbenzene, and xylene compounds in ambient urban atmosphere in Ahvaz, Iran. *Archives of Hygiene Sciences* 9(2): 152-167 (2020).
14. F. Borhani, M.S.Motlagh, A.H. Ehsani, Y. Rashidi, M. Ghahremanloo, M. Amani, and A. Moghimi. Current status and future forecast of short-lived climate-forced ozone in Tehran, Iran, derived from ground-based and satellite observations. *Water, Air, & Soil Pollution* 234(2): 134 (2023).
15. F. Borhani, A.H. Ehsani, S.L. McGuirk, M.S. Motlagh, S.M. Mousavi, Y. Rashidi, and S.M. Mirmazloumi. Examining and predicting the influence of climatic and terrestrial factors on the seasonal distribution of ozone column depth over Tehran province using satellite observations. *Acta Geophysica* 72(2): 1191-1226 (2024).
16. GIOVANNI: NASA's Goddard Earth Sciences Data and Information Services Center. *NASA: Earthdata* (2022). https://giovanni.gsfc.nasa.gov/giovanni/
17. F. Borhani, A.A. Pourezzat, and A.H. Ehsani. Spatial distribution of Particulate Matter in Iran from Internal factors to the role of western adjacent countries from political governance to Environmental Governance. *Earth Systems and Environment* 8(1): 135-164 (2024).
18. F. Borhani and A. Noorpoor. Cancer risk assessment Benzene, Toluene, Ethylbenzene and Xylene (BTEX) in the production of insulation bituminous. *Environmental Energy and Economic Research* 1(3): 311-320 (2017).
19. U.S. EPA. Exposure Factors Handbook (1997, Final Report). *U.S. Environmental Protection Agency, Washington, DC*, EPA/600/P-95/002F a-c, (1997). https://cfpub.epa.gov/ncea/efp/recordisplay.cfm?deid=12464
20. U.S. EPA. Exposure Factors Handbook 2011 Edition (Final Report). *U.S. Environmental Protection Agency, Washington, DC*, EPA/600/R-09/052F, (2011). https://cfpub.epa.gov/ncea/efp/recordisplay.cfm?deid=236252
21. A.H. Sial, S.Y.S. Rashdi, and A.H. Khan. Comparative analysis of data visualization libraries Matplotlib and Seaborn in Python. *International Journal of Advanced Trends in Computer Science and Engineering* 10(1): 277-281 (2021).
22. L.A.J. Bastien, N.J. Brown, and R.A. Harley. Contributions to local-and regional-scale formaldehyde concentrations. *Atmospheric Chemistry and Physics* 19(13): 8363-8381 (2019).
23. G.P. Ayers, R.W. Gillett, H. Granek, C. De Serves, and R.A. Cox. Formaldehyde production in clean marine air. *Geophysical Research Letters* 24(4): 401-404 (1997).
24. K. Müller. Determination of aldehydes and ketones in the atmosphere - A comparative long time study at an urban and a rural site in eastern Germany. *Chemosphere* 35(9): 2093-2106 (1997).
25. Y. Zhang, R. Li, Q. Min, H. Bo, Y. Fu, Y. Wang, and Z. Gao. The controlling factors of atmospheric formaldehyde (HCHO) in Amazon as seen from satellite. *Earth and Space Science* 6(6): 959-971 (2019).
26. T. Liu, Y. Lin, J. Chen, G. Chen, C. Yang, L. Xu, M. Li, X. Fan, Y. Chen, L. Yin, Y. Chen, X. Ji, Z. Lin, F. Zhang, H. Wang, and Y. Hong. Seasonal characteristics of atmospheric formaldehyde (HCHO) in a coastal city of southeast China: Formation mechanism and photochemical effects. *Atmospheric Chemistry and Physics* 2022: 1-28 (2022). https://doi.org/10.5194/acp-2022-292
27. F. Vichi, C. Bassani, A. Ianniello, G. Esposito, M. Montagnoli, and A. Imperiali. Formaldehyde Continuous Monitoring at a Rural Station North of Rome: Appraisal of Local Sources Contribution and Meteorological Drivers. *Atmosphere* 14(12): 1833 (2023).
28. M. Hu, Y. Wang, S. Wang, M. Jiao, G. Huang, and B. Xia. Spatial-temporal heterogeneity of air pollution and its relationship with meteorological factors in the Pearl River Delta, China. *Atmospheric Environment* 254: 118415 (2021).
29. S.K. Kuhpar, G. Janbazghobadi, and S. Motevali. Spatial Analysis of Bioclimatic Vulnerability of heat wave hazard in Ahwaz city Pilot. *Journal of Climate Research* 1400(48): 85-98 (2022).
30. J. Kuttippurath, K. Abbhishek, G.S. Gopikrishnan, and M. Pathak. Investigation of long–term trends and major sources of atmospheric HCHO over India. *Environmental Challenges* 7: 100477 (2022).
31. S. Dhankar and B. Pani. Spatio-temporal analysis of formaldehyde and its association with atmospheric and environmental variables over the Southeast Asian region using satellite data. *Environmental Monitoring and Assessment* 197(2): 185 (2025).

Appendix

Table A. Monthly average of formaldehyde (HCHO), other air pollutants (CO, NO_2, O_3, SO_2) and meteorological parameters recorded from 2019 to 2022 in Ahvaz, Iran.

Year	Month	HCHO ($\frac{mol}{m^2}$)	Other air pollutants				Meteorological Parameters				
			CO ($\frac{mol}{m^2}$)	NO_2 ($\frac{mol}{m^2}$)	O_3 ($\frac{mol}{m^2}$)	SO_2 ($\frac{mol}{m^2}$)	T (°C)	WS ($\frac{m}{s}$)	RH (%)	DWP (°C)	PP ($\frac{kgr}{m^2 s}$)
2019	Jan	0.00005	0.033714	0.00012	0.113483	0.000219	13.7373	5.3063	131.1563	6.5750	0.0258
	Feb	0.0001178	0.035167	0.000184	0.124667	0.00031	14.7604	5.0131	118.5313	5.4111	0.0128
	Mar	0.000104	0.035087	0.000106	0.140444	0.000192	17.7945	5.4235	103.2500	6.6703	0.0264
	Apr	0.0001396	0.036577	0.000129	0.136647	0.000291	23.4250	5.1949	92.6406	10.1673	0.0092
	May	0.0001778	0.035143	0.000121	0.134667	0.000315	32.6782	5.0413	49.5156	10.9966	0.0007
	Jun	0.0002258	0.034067	0.000161	0.128571	0.000301	39.1134	6.3854	34.8828	6.7054	0.0000
	Jul	0.0002302	0.033379	0.000109	0.129361	0.000153	39.0319	7.7749	34.1953	4.0256	0.0001
	Aug	0.000258	0.035539	0.000136	0.129	0.000381	39.9686	5.9878	40.7266	6.1979	0.0000
	Sep	0.0001933	0.032179	0.000117	0.122714	0.000265	36.9697	6.2034	41.2656	2.8213	0.0000
	Oct	0.000188	0.032423	0.000113	0.12273	0.000414	31.4266	4.5068	74.0313	7.8402	0.0154
	Nov	0.0001636	0.033214	0.000165	0.127	0.000536	20.9432	3.5398	101.0938	6.1633	0.0117
	Dec	0.000087	0.0322	0.000149	0.132618	0.000868	15.7801	4.3359	137.7500	7.8929	0.0270
2020	Jan	0.0000886	0.035613	0.000134	0.142514	0.000716	13.6067	4.5294	120.3438	4.6372	0.0145
	Feb	0.0000868	0.035037	0.000113	0.136364	0.000485	15.9229	5.0808	112.8750	4.7152	0.0299
	Mar	0.0001208	0.03644	0.000112	0.138971	0.000497	19.7665	4.9384	97.4688	7.8149	0.0253
	Apr	0.0001375	0.037138	0.000096	0.14	0.000362	25.4150	5.7123	77.8594	9.6308	0.0084
	May	0.000194	0.037371	0.000115	0.130865	0.00031	33.2430	5.5274	47.9297	6.1069	0.0007
	Jun	0.0002061	0.033455	0.000102	0.123714	0.000167	37.7906	7.6587	32.3203	2.1011	0.0000
	Jul	0.0002703	0.034625	0.000114	0.125135	0.000336	41.3702	5.7505	39.6719	6.9508	0.0000
	Aug	0.0002294	0.032375	0.000159	0.123857	0.00026	38.4803	6.7521	42.6563	3.7184	0.0000
	Sep	0.0002625	0.0345	0.000137	0.12325	0.000503	37.5153	4.9809	45.6250	5.0284	0.0001
	Oct	0.0001905	0.035471	0.000152	0.118135	0.000363	30.2534	4.3010	55.9531	-2.4697	0.0000
	Nov	0.0001513	0.033192	0.000117	0.122343	0.000439	21.8479	4.7806	113.1875	9.4163	0.0471
	Dec	0.000083	0.033731	0.000102	0.127486	0.00059	15.0287	4.2652	134.6875	7.3165	0.0211

2021	Jan	0.000124	0.035931	0.000235	0.126784	0.000806	14.8778	4.0707	112.5625	3.2985	0.0042
	Feb	0.000087	0.034407	0.000133	0.128394	0.000475	16.8723	4.6399	104.5000	4.3241	0.0134
	Mar	8.48E-05	0.036633	0.0001	0.132649	0.000196	21.0888	5.3366	84.3438	4.6515	0.0058
	Apr	0.000148	0.0362	0.000112	0.134	0.00031	28.9377	5.2291	57.3828	4.0214	0.0011
	May	0.000203	0.03529	0.000134	0.135973	0.000281	35.6096	5.9196	40.9922	2.5787	0.0006
	Jun	0.000198	0.032452	0.000112	0.128382	0.000229	38.7664	7.7936	31.9453	-1.0558	0.0004
	Jul	0.000216	0.034162	0.000121	0.130595	0.000267	41.1648	6.7086	35.6875	4.6762	0.0003
	Aug	0.00023	0.038242	0.000125	0.130757	0.000321	40.1211	5.4004	37.1172	5.7986	0.0001
	Sep	0.000179	0.034882	0.000129	0.127314	0.000236	35.6297	6.2035	42.2734	1.7389	0.0000
	Oct	0.00014	0.032771	0.000119	0.123081	0.000224	30.8433	5.4585	54.7813	0.1899	0.0008
	Nov	0.000144	0.032618	0.000127	0.127278	0.000436	23.0375	4.5013	94.8594	6.5484	0.0073
	Dec	0.000116	0.033304	0.000127	0.127441	0.000643	16.6429	5.0100	119.9063	5.4328	0.0216
2022	Jan	0.000074	0.033407	0.000159	0.129944	0.00081	13.0508	4.1429	126.9063	2.5020	0.0133
	Feb	9.01E-05	0.033929	0.000167	0.132647	0.00039	16.9183	5.0328	111.2188	3.7435	0.0129
	Mar	8.55E-05	0.035591	0.0001	0.134081	0.000205	19.9233	5.4765	88.7344	1.0220	0.0092
	Apr	0.00012	0.034333	0.000135	0.140571	0.000246	28.8860	4.9800	63.9063	1.1829	0.0059
	May	0.000144	0.033387	0.000101	0.129054	0.000136	31.9898	6.8086	46.5703	0.7040	0.0008
	Jun	0.000196	0.034844	0.000134	0.132471	0.000269	39.4897	6.6747	33.7188	1.0517	0.0001
	Jul	0.000246	0.035677	0.000129	0.131083	0.000299	39.7620	6.4188	42.7578	4.8379	0.0024
	Aug	0.00028	0.035606	0.000149	0.131361	0.00041	40.6584	5.1017	46.5547	7.7839	0.0004
	Sep	0.000236	0.033824	0.000135	0.127306	0.000498	36.4741	4.8781	47.1172	2.8872	0.0000
	Oct	0.000184	0.033367	0.000103	0.121649	0.000497	32.4669	4.2601	51.2188	2.0484	0.0006
	Nov	0.00015	0.02944	0.000141	0.129571	0.000357	23.0908	4.6627	103.4688	8.8915	0.0132
	Dec	0.000101	0.031133	0.000163	0.130686	0.000718	16.7387	4.4562	124.4375	5.9849	0.0220